IRIS AperTO

UNIVERSITÀ DEGLI STUDI DI TORINO

AperTO - Archivio Istituzionale Open Access dell'Università di Torino

Ab Initio Periodic Simulation of the Spectroscopic and Optical Properties of Novel Porous Graphene Phases

This is the author's manuscript

Original Citation:

Availability:

This version is available http://hdl.handle.net/2318/130959 since 2016-09-13T17:26:25Z

Published version:

DOI:10.1021/jp3103436

Terms of use:

Open Access

Anyone can freely access the full text of works made available as "Open Access". Works made available under a Creative Commons license can be used according to the terms and conditions of said license. Use of all other works requires consent of the right holder (author or publisher) if not exempted from copyright protection by the applicable law.

(Article begins on next page)

12 October 2024

Ab initio periodic simulation of the spectroscopic and optical properties of novel porous graphene phases

Marco De La Pierre,[*,†] Panaghiotis Karamanis,[‡] Jacopo Baima,[†] Roberto Orlando,[†] Claude Pouchan,[‡] and Roberto Dovesi[†]

Dipartimento di Chimica, Università di Torino and NIS -Nanostructured Interfaces and Surfaces - Centre of Excellence, http://www.nis.unito.it, Via P. Giuria 7, 10125 Torino, Italy, and Equipe de Chimie Physique, IPREM UMR5254, Université de Pau et des Pays de l'Adour, 64000 Pau, France

E-mail: marco.delapierre@unito.it

KEYWORDS: porous graphene, infrared spectrum, raman spectrum, vibrational frequencies, intensities, polarizability, hyperpolarizability, CPHF/CPKS, quantum mechanical calculations, CRYSTAL code

[*]To whom correspondence should be addressed

[†]Dipartimento di Chimica, Università di Torino and NIS -Nanostructured Interfaces and Surfaces - Centre of Excellence, http://www.nis.unito.it, Via P. Giuria 7, 10125 Torino, Italy

[‡]Equipe de Chimie Physique, IPREM UMR5254, Université de Pau et des Pays de l'Adour, 64000 Pau, France

Abstract

We present a detailed periodic *ab initio* quantum-mechanical simulation of two recently proposed systems, namely hydrogenated porous graphene (HPG) and biphenyl carbon (BPC), using hybrid HF-DFT functionals and all-electron Gaussian-type basis sets. The equilibrium geometry, the vibrational spectrum (including IR intensities), the full set of components of the polarizability and hyperpolarizability tensors are provided, the latter evaluated through a Coupled-Perturbed KS/HF scheme. IR and Raman spectra for the two systems are quite different, and differ also from graphene, thus permitting their experimental identification. It is then shown that small defects inserted into the graphene sheet lead to finite values for the in-plane components of the static (hyper)polarizability tensors, spanning a relatively large range of values. By dehydrogenation of porous graphene into biphenyl carbon, a noteworthy enhancement of the non-linear optical properties through the static second dipole hyperpolarizability can be achieved. Vibrational contributions to the polarizability are negligible for both systems.

1 Introduction

One of the most captivating collateral scientific breakthroughs triggered by studies on single sheets of graphite, widely known as graphene,[1,2] is the rise of a new revolutionary class of one-atom-thick "wonder materials".[3] Starting from graphene one can obtain new 2D materials simply by "drilling holes" on its honeycomb structure or by synthesizing, with atomic precision[4] and a bottom-up approach, systems bearing controllable "defects" (pores) on their structure. In this fashion one may alter, enhance, or even tune some of the desired properties. Such 2D graphene-like networks may maintain some of the outstanding intrinsic physical properties of graphene (superior electrical and thermal conductivity, extraordinary strength etc)[5–7] fitting at the same time in new feasible applications.[8] For instance, it is now known that one can open the zero-band gap of graphene by simply introducing pores in its network, making it suitable for applications in electronics.[9] Alternately, pierced graphene membranes might be developed as molecular filters,[10] energy[11] and hydrogen[12] stores or even as micro distillers.[13]

Motivated by the above list of promising developments, we here report a quantum-mechanical study of two representative graphene-like systems that have recently been the subject of several attention-grabbing studies. The first of these carbon phases, recently synthesized by Bieri et al.,[4] is perhaps the most obvious periodic pores-bearing hydrogenated graphene system (HPG) with single-atom-wide spatial gaps (see Figure 1(a)). HPG, a 2D covalently bonded molecular network of polyphenylene forming a polyphenylene superhoneycomb, has already attracted considerable attention due to its particular electronic and physical properties.[12]

The second system we consider here is biphenylene carbon (BPC), whose structure is shown in Figure 1(b). This hydrogen-free 2D network of carbon atoms has been described by Baughman et al.,[14] long before the discovery of graphene, as a possible (but not favorable) product of the cyclotrimerization of graphyne. However, only after being recently classified as one of the potential "graphene allotropes"[15] it has caught particular attention. What is exciting about these two systems is the fact that BPC can be obtained from HPG, as recently suggested by Brunetto et al.[16] by means of ab-initio molecular dynamics, where BPC would be spontaneously formed after selective dehydrogenation of HPG. In contrast to pristine graphene this new "graphene allotrope" is characterized by non-zero band gap while in comparison with HPG it bears extensively delocalized π-orbitals.

The purpose of this work is to provide accurate structural and detailed spectroscopic data for the above described "graphene phases", by means of all-electron periodic calculations. Such information is of essential importance for their characterization, that might prove valuable in their further experimental identification. Of our particular interest is also to investigate how the zero-band gap breach of pristine graphene (achieved by introducing small one-atom-wide defects) influences its optical properties, and also how these properties change when HPG is transformed to conjugated PBC. Understanding the basis of the dipole (hyper)polarizabilities in periodic graphene-like systems is of critical importance due to the increasing interest in the non-linear optical response properties (NLO) of graphene and its possible use in photonic and optoelectronic applications.[17,18] Extraordinary graphene features such as saturable absorption, fast and high quadratic electro-optic

effect (Kerr effect) and coherent ultra-broadband nonlinear optical response[19–21] leave plenty of promises in upgrading current photonic technologies. At the same time its particular two-dimensional structure with exotic electronic and magnetic properties[22] might provide the fertile ground for further innovations in impending photonic technologies at the nano-scale.[23]

2 Computational Method

Calculations were performed with the CRYSTAL09 periodic *ab initio* code,[24,25] by using an all-electron Gaussian-type basis set and the B3LYP hybrid functional[26–28] that has recently been applied to the study of structural, vibrational and optical properties of semiconducting C and BN nanostructures.[29–33] Hybrid functionals have been reported to be more accurate than both Hartree-Fock and pure DFT approaches in the simulation of static polarizability and first hyper-polarizabilities of solids.[34,35] Moreover, B3LYP has been proven to be one of the most accurate functionals in the simulation of the vibrational properties of solids.[36]

Carbon and hydrogen were described by 6-31G(2d) and 311G(2p)contractions, respectively, that have recently been adopted for the study of other carbon compounds with similar chemistry, such as nanotubes[30] and polyacetylene.[37,38] These basis sets were derived from standard molecular basis sets, through re-optimization of the most diffuse functions according to the variational principle; the resulting exponents (in bohr^{-2}) are $\alpha_{sp} = 0.190$ and $\alpha_d = 0.400$ for C and $\alpha_s = 0.103$ and $\alpha_p = 0.375$ for H.

It is well known that basis set is a very important issue in the calculation of the (hyper)polarizabilities,[39–41] especially for non-3D periodic systems. In particular, it has been shown[38] that the (hyper)polarizabilities of 1D-periodic polyacetylene chains can be computed with great accuracy by adding nets of ghost functions along the non-periodic directions; the resulting accuracy is comparable with the one obtained in molecular calculations for oligomer chains described with polarizability-specific, diffuse functions-enriched basis sets. Starting from the standard basis set adopted in this paper (BS A), we built three more basis sets. In the case of BS B, we added two layers of s ghost functions

($\alpha_s = 0.15$), parallel to the atomic plane, at a z distance of +1.5 and -1.5 Å, respectively: for each atom of the structure, two ghost functions were added with the same x,y coordinates and with a shifted z coordinate. Note that for BPC a s ghost function was added in the center of the 12-C ring as well, the distance from C atoms being 2.74 Å; functions at $z = \pm 1.5$ Å from this in-layer ghost were added, too. BS C contains 4 ghost layers in total, at z distances of ± 1.5 and ± 3.0 Å from the atomic plane; finally, BS D contains 2 additional ghost layers (6 in total) at a z distance of ± 4.5 Å. See Ref.[38] for more details on the use of ghost functions in (hyper)polarizability calculations.

The level of accuracy in evaluating the bielectronic Coulomb and Hartree-Fock exchange series is controlled by five parameters T_i ($i = 1, ...5$).[24] T_1 and T_2 refer to the Coulomb integrals, T_3, T_4 and T_5 to the exchange ones: integrals are either approximated or disregarded when the *overlap* between the corresponding basis functions is below 10^{-T_i}. More details on these truncation criteria can be found in Refs.[24,37] . Following the guidelines proposed in Ref.[37] the values of 9, 9, 9, 30, 60 were chosen. The threshold on the SCF energy was set to 10^{-9} Ha for geometry optimization and to 10^{-10} Ha for the calculation of vibrational frequencies and (hyper)polarizabilities. The reciprocal space was sampled along the 2 lattice vectors according to a sublattice with shrinking factor[24] set to 12 for HPG and BPC and to 56 for graphene, corresponding to 19 and 290 independent $\vec{k}$ vectors in the irreducible part of the Brillouin zone, respectively. The conducting nature of a graphene sheet required a denser net of $\vec{k}$ points and more severe conditions for the thresholds to ensure convergence of the exchange series (a fraction of which appears in hybrid functionals).

The DFT exchange-correlation contribution is evaluated by numerical integration over the unit cell volume. In CRYSTAL, radial and angular points of the grid are generated through Gauss-Legendre radial quadrature and Lebedev two-dimensional angular point distributions. A (75,974)p grid was used, corresponding to a pruned grid with 75 radial and 974 angular points (XLGRID keyword in the CRYSTAL09 manual[24]). Accuracy of this grid can be estimated from the error on the integrated electronic charge density in the unit cell, that amounts to less than 0.0003% for BPC and is even smaller for HPG and graphene.

Structures were optimized by using the analytical energy gradients with respect to atomic coordi-

nates and unit cell parameters,[42–44] within a quasi-Newtonian scheme combined with the BFGS algorithm for Hessian updating.[45–48] Convergence was checked on both gradient components and nuclear displacements, for which default values[24] were chosen.

The calculation of vibrational frequencies at the Γ point, $\nu_{0,n}$, was performed within the harmonic approximation. Frequencies are obtained by diagonalizing the mass-weighted Hessian matrix W, which is constructed by numerical differentiation of the analytical gradients with respect to the atomic Cartesian coordinates:

$$W_{\alpha i,\beta j}(\vec{k}=\vec{0}) = \frac{1}{\sqrt{M_\alpha M_\beta}} H_{\alpha i,\beta j} \tag{1}$$

where $H_{\alpha i,\beta j}$ is the second derivative of energy (evaluated numerically starting from the analytical gradients), M_α and M_β are the atomic masses; greek and latin indices refer to atoms and atomic Cartesian coordinates, respectively. The calculated (optimized) equilibrium geometry was taken as reference.

Integrated intensities for IR absorption, II_n, were computed for each $n-th$ mode by means of the mass-weighted effective mode Born charge vector,[49,50] $\vec{Z}_n = \frac{\partial}{\partial Q_n}\vec{\mu}$, evaluated through the Berry phase approach:[51–53]

$$II_n = \frac{1}{4\pi\varepsilon_0}\frac{\pi}{3}\frac{N_A}{c^2}\cdot d_n \cdot \left|\vec{Z}_n\right|^2 \tag{2}$$

where ε_0 is the vacuum dielectric permittivity ($1/4\pi\varepsilon_0$ = 1 atomic unit), N_A is the Avogadro's number, c is the speed of light, d_n is the degeneracy of the $n-th$ mode, $\vec{\mu}$ is the cell dipole moment and Q_n is the normal mode displacement coordinate. Details on the calculation of vibrational frequencies and infrared intensities can be found in Refs.[54–56]

Electronic contributions to the static polarizability and hyperpolarizabilities were evaluated through a Coupled-Perturbed KS/HF (Kohn-Sham/Hartree-Fock) scheme[57] as adapted to periodic systems.[58] This self-consistent method focuses on the description of the Crystalline Orbital relaxation under the effect of an external electric field. Perturbed wavefunctions are then used to calculate the

dielectric properties as energy derivatives. More details about the method and its implementation in the CRYSTAL code can be found in Refs.[31–33,59–64]

The total static polarizability tensor α was obtained as the sum of the electronic and vibrational contributions:

$$\alpha_{ij} = \alpha_{el,ij} + \alpha_{vib,ij} = \alpha_{el,ij} + \frac{1}{4\pi\varepsilon_0} \sum_n \frac{\vec{Z}_{n,i}\vec{Z}_{n,j}}{\nu_{0,n}^2} \tag{3}$$

where $\vec{Z}_n$ are the mass-weighted Born charges and $\nu_{0,n}$ the corresponding vibrational frequencies.

A graphical representation of the infrared spectrum $S(\nu)$ was obtained as a superposition of Lorentzian functions F, one for each mode:

$$S(\nu) = \sum_n F(\nu; \nu_{0,n}, II_n, \gamma_n) \tag{4}$$

$$F(\nu; \nu_{0,n}, II_n, \gamma_n) = \frac{II_n}{\pi} \left[\frac{\gamma_n/2}{(\nu - \nu_{0,n})^2 + \gamma_n^2/4} \right] \tag{5}$$

where γ_n is the damping factor of the $n-th$ mode, which is related to the phonon lifetime. Being unable to compute this quantity, we used a constant value of 8 cm^{-1} (see Ref.[65]). $S(\nu)$ curves were evaluated in the range of 0-1100 cm^{-1}, in steps of 1 cm^{-1}.

Graphical animations of the normal modes are available at the CRYSTAL Web site (`www.crystal.unito.it/prtfreq/jmol.html`); they provide a simple and intuitive interpretation of the "nature" of the modes (stretching, bending, rotation, translation, etc).

Manipulation and visualization of structures were performed with the Jmol 3D engine (`jmol.sourceforge.ne` `www.theochem.unito.it/ crystal_tuto/mssc2008_cd/ tutorials/webvib/index.html`

Molecular drawings were rendered with the Inkscape program (`www.inkscape.org`) using input files prepared with Jmol. Data analysis was performed using the LibreOffice suite (`www.libreoffice.org`

Graphs were realized with the Gnuplot utility (`www.gnuplot.info`).

3 Results and Discussion

3.1 Structure and stability

An overall view of the layer structure of HPG (hydrogenated porous graphene) and BPC (biphenyl carbon) is given in Figure 1; the unit cells are represented in both planar (Figure 1) and tilted (Figure 2) views. Structural parameters are reported in Table 1. Both compounds can be described as "porous" graphene-like sheets, with pores defined by rings of either 6 C_3-H groups (HPG, 2 C atoms being shared between 2 rings) or 12 C atoms (BPC); in both cases there is one pore per unit cell.

From a crystallographic point of view, the unit cell of both HPG and BPC can be compared to a 3x3 graphene supercell. In HPG, the structure can be described as a network of C_6H_3 benzene-like units, inter-connected through C-C bonds. The cell parameter is 7.46 Å (1% larger than graphene). Bond distances in the benzene-like unit are 1.40 Å for C-C (the same as in actual benzene molecule) and 1.08 Å for C-H; C-C bonds connecting pairs of units are larger, 1.49 Å (a typical value for single C-C bonds). Steric repulsion between H atoms induces a symmetry lowering with respect to a graphene sheet. The resulting space group is *C*222, due to the tilting of the C_6H_3 units with respect to the sheet plane by an angle of 10.45 degrees. H-H distances are 1.95-2.05 Å (they are 1.87 Å if the system is constrained to be planar).

Other reported values for the HPG cell parameter are 7.45 Å (HSE06 hybrid functional[66]) and 7.52-7.53 Å (BLYP pure GGA functional[16]). The experimental value is 7.4 Å,[4] which is comparable with the values obtained with both B3LYP (present study) and HSE06[66] functionals.

BPC preserves the full graphene symmetry and a perfect planar structure, with a cell parameter reduced to 6.75 Å. Three types of rings make up the sheet, formed by 4, 6 and 12 C atoms. The square 4-C rings have 1.47-1.48 Å C-C distances, and obviously represent a severe constraint for the structure, with angles of 90.0 degrees highly distorted for sp^2 hybridization. 12-C rings alternate 1.36 and 1.48 Å C-C distances, and show (again distorted) angles of 150.0 degrees; note the large diameter of 5.49 Å. Finally, the hexagonal 6-C rings show sp^2-typical angles of 120.0

degrees and alternated C-C distances of 1.36 and 1.47 Å.

We were unable to find information on actual synthesis of BPC. The BLYP work by Brunetto et al.[16] gives values of 6.69 and 6.78 Å for *a* and *b*, respectively, close to the value proposed in this study. Semi-empirical methods provide values in worse agreement: MNDO[14] and tight binding[15] provide 6.63 and 6.83 Å, respectively.

When compared to graphene and molecular H_2, HPG is less stable by 0.099 eV per $CH_{\frac{1}{2}}$ unit. However, if reference is made to atomic H, HPG formation is favored by 1.097 eV per $CH_{\frac{1}{2}}$ unit. Thus, synthesis of this compound is likely to occur in an atmosphere of atomic H.

Concerning BPC, it is 0.658 eV per C atom less stable than graphene. Specific reaction pathways should then be designed, to avoid use of pure graphene as the reactant. This value is in quite close agreement with the value of 0.63 eV/atom obtained with the BLYP functional.[16] A tight binding study[15] resulted in a larger formation energy (0.828 eV/atom).

3.2 Electronic structure

The band structure for graphene, HPG and BPC is shown in Figure 3. Values for the band gap are reported in the last row of Table 2.

In all the three cases, the band gap is direct and lies at *K* point in the first Brillouin zone. Graphene, BPC and HPG have gap values of 0, 1.08 and 3.95 eV, respectively. The large band gap of HPG can be related with its peculiar aromatic structure. Resonant π bonds are present only inside the benzene-like rings; single C-C bonds that interconnect rings isolate their aromatic units, hindering electron delocalization on the whole structure (contrary to both cases of graphene and BPC).

The BLYP study by Brunetto et al.[16] gives values of 0.8 and 3.3 eV for BPC and HPG, respectively, which are about 20% smaller than our results. This is reasonable, as pure GGA functionals are known to underestimate experimental band gap values, while hybrid functionals are usually closer to experiments.[67,68] A similar value for HPG, 3.2 eV, has been reported by Du et al.[66] for a calculation with the HSE06 hybrid functional, in agreement with the relative performances of hybrid functionals published in the literature.[69] For the same system, these authors also reported

an even smaller value, 2.34 eV, obtained at the LDA level.

3.3 Vibrational properties

The computed vibrational properties for both HPG and BPC are listed in Table 3; a graphical representation of the infrared (IR) spectra is given in Figure 4.

As regards HPG, all 51 vibrational modes are non-degenerate (i.e. have one-dimensional IRREPs). All of them are Raman active, while only 39 are IR active. Let us concentrate on the latter, for which also the IR intensities are available. Frequencies of modes with intensity higher than 10 km/mol are in bold in Table 3. They correspond to the intense IR peaks of Figure 4. Graphical animation of the modes helps in assigning these modes to the corresponding lattice motions. Among the intense modes, the ones at 651.9-654.8 cm^{-1} are the only ones which involve pure C motions (contraction of the C_6H_3 units). The modes at 882.9, 926.5 and 934.0 cm^{-1} are related to out-of-plane C-H bending, while all the other intense modes below 1700 cm^{-1} (1147.1, 1150.6, 1384.7, 1391.2, 1630.2 and 1631.0 cm^{-1}) are related to in-plane C-H bending coupled with C_6H_3 ring breathing. As expected, high frequency modes at 3218.5 and 3232.2 cm^{-1} are C-H stretchings.

BPC has 22 vibrational modes (11 non-degenerate and 11 two-fold degenerate modes). Among them, 3 are IR active and 8 are Raman active. The IR spectrum (Figure 4) features two highly intense modes at 823.4 and 1267.0 cm^{-1}.

The IR spectra of the two compounds are quite different from each other, whereas graphene has no IR active modes. Therefore, HPG and BPC should be clearly recognizable upon IR experimental characterization.

3.4 Polarizability and hyperpolarizabilities

Computed static electronic polarizability and hyperpolarizabilities are given in Table 2; data for graphene are also shown for comparison; as in the case of structural properties, all values refer to unit cells of comparable size as given in Table 1 (3x3 supercell for graphene).

In-plane (x,y) polarizability is correlated to the inverse of the electronic band gap (see Section 3.2):

the α_{xx} value in graphene, BPC and HPG is infinite, 719 and 324 bohr^3, respectively. Out-of-plane polarizability α_{zz} is similar for the three systems: 52 (graphene), 50 (HPG) and 40 (BPC) bohr^3, and much smaller than α_{xx}, as expected.

All first order hyperpolarizabilities β are 0 both in graphene and in BPC, due to inversion symmetry. In the case of HPG a small β_{xyz} value appears (20 a.u.).

As regards second hyperpolarizabilities γ, in graphene there are 5 tensorial components that go to infinity, namely axial γ_{xxxx} ($= \gamma_{yyyy}$) and transversal ones γ_{xxyy}, γ_{xxzz} and γ_{yyzz}. The only other non-null component is the out-of-plane γ_{zzzz}, wich has a value of $2.56 \cdot 10^3$ a.u..

Due to the non-zero gap, all the γ components are finite in both HPG and BPC. In-plane components are in the range 10^5-10^7 a.u.. Notably, γ_{xxxx}, γ_{yyyy} and γ_{xxyy} increase by a factor of 33, 26 and 28, respectively, when going from HPG to BPC; this trend correlates to the smaller band gap of the latter compound. According to Brunetto et al.,[16] BPC can in principle be obtained from HPG by simple selective dehydrogenation. Then, this can represent a way to tune the hyperpolarizabilities of graphene-like sheets by the large factors given above.

Partially out-of-plane components (γ_{xxzz}, γ_{yyzz}) are of the same order of magnitude, 10^3 a.u., for both HPG and BPC. Similarly, the pure out-of-plane component γ_{zzzz} is $4.66 \cdot 10^3$ and $2.80 \cdot 10^3$ a.u. for HPG and BPC, respectively. The former value is 80% larger than for graphene, while the latter is about the same.

Let us now discuss the effect of the basis set in the case of BPC (hyper)polarizabilities, by taking BS A as a starting point (see Table 4). The α polarizability increases by 3% and 40% (in-plane and out-of-plane components) when 2 ghost layers (BS B) are added. When more ghost layers are added, these values remain unchanged to within 1%. Thus, α is very accurately described with only 2 additional ghost layers. A similar consideration holds for the in-plane hyperpolarizabilities γ_{xxxx} and γ_{xxyy} (here the effect of adding the first 2 layers is a 10% increase).

The situation is more delicate in the case of the out-of-plane hyperpolarizabilities. The mixed component γ_{xxzz} increases by 480%, 8% and 3% when adding 2, 4 and 6 ghost layers, respectively. From this trend BS D is expected to differ by less than 1% from the fully converged result. The

perpendicular component γ_{zzzz} is the most sensitive to the basis set. Its value is about 0 when no ghost functions are used; it raises to 1401 with BS A, and to 2410 (+72%) and 2796 (+16%) with BS C and BS D, respectively. BS D is then expected to differ by 3-4% from the fully converged result.

Due to the computational cost (an increase by a factor 30 from BS A to BS D is observed), we did not go beyond basis set D, that was then adopted to compare electronic polarizability and hyperpolarizabilities of graphene, HPG and PBC.

Vibrational contributions to the static polarizability (not reported in Table 2) are almost negligible, as expected for apolar systems. In-plane components are equal to 8.6 ($\alpha_{vib,xx}$) and 10.5($\alpha_{vib,yy}$) bohr^3 for HPG and to 7.6 ($\alpha_{vib,xx}$=$\alpha_{vib,yy}$) bohr^3 for BPC; the out-of-plane component $\alpha_{vib,zz}$ is 1.2 (HPG) and 0.0 (BPC) bohr^3. For graphene, $\alpha_{vib,xx}$=$\alpha_{vib,yy}$=$\alpha_{vib,zz}$=0, as there are no IR active modes.

To the best of our knowledge, there are neither experimental nor computational studies in the literature reporting values of (hyper)polarizabilities for HPG and BPC. Here, let us recall that the B3LYP functional provides rather accurate values for the electronic band gap (see Section 3.2, and Refs.[67–69]), which is a very important element for the evaluation of polarizability and hyperpolarizabilities in a perturbative treatment.[37]

4 Conclusions

Relying on all-electron hybrid density functional periodic computations we have studied the structural, electronic, spectroscopic and (linear and non-linear) optical properties of two graphene phases. Detailed information about the equilibrium geometries, band gaps and spectroscopic data of hydrogenated porous graphene and graphene-biphenyl carbon are reported and compared with those of earlier studies. In addition, reference hybrid HF-DFT analytical values of the dipole polarizabilities and hyperpolarizabilities are given.

The obtained results demonstrate how the opening of a band gap in the graphene sheet affects its

static dipole (hyper)polarizabilities. Also, it is shown that the transformation of porous graphene to BPC by selective dehydrogenation (an energy barrier-free reaction, according to Brunetto et al.[16]) is followed by a significant increase in its dipole polarizability (more than 100%) and by a dramatic enhancement of its second hyperpolarizability. For the latter property our results predict that the hyperpolarizability in each direction of the plane increases by a factor around 30 after the transformation of HPG to BPC.

The remarkable change in the second hyperpolarizability is mainly explained in terms of extensive conjugation in the BPC framework, which is destroyed in hydrogen saturated HPG. Hence, by dehydrogenating porous graphene one can achieve a noteworthy enhancement of its non-linear optical properties, described by its microscopic static second dipole hyperpolarizability. Apparently, as in simple organic molecules and polymers, our results confirm that conjugation is of primary importance for the magnitude of the second hyperpolarizability in 2D graphene-like networks.

To our knowledge this is the first time that (hyper)polarizabilities of such graphene-based systems are reported at the infinite periodic limit. Our contribution can be used as a reference for computations that might target smaller finite graphene systems (flakes or ribbons) bearing similar structural features.

Acknowledgement

The authors acknowledge Compagnia di San Paolo for financial support (Progetti di Ricerca di Ateneo-Compagnia di San Paolo-2011-Linea 1A, progetto ORTO11RRT5). Computer support from the CINECA supercomputing centre is kindly aknowledged.

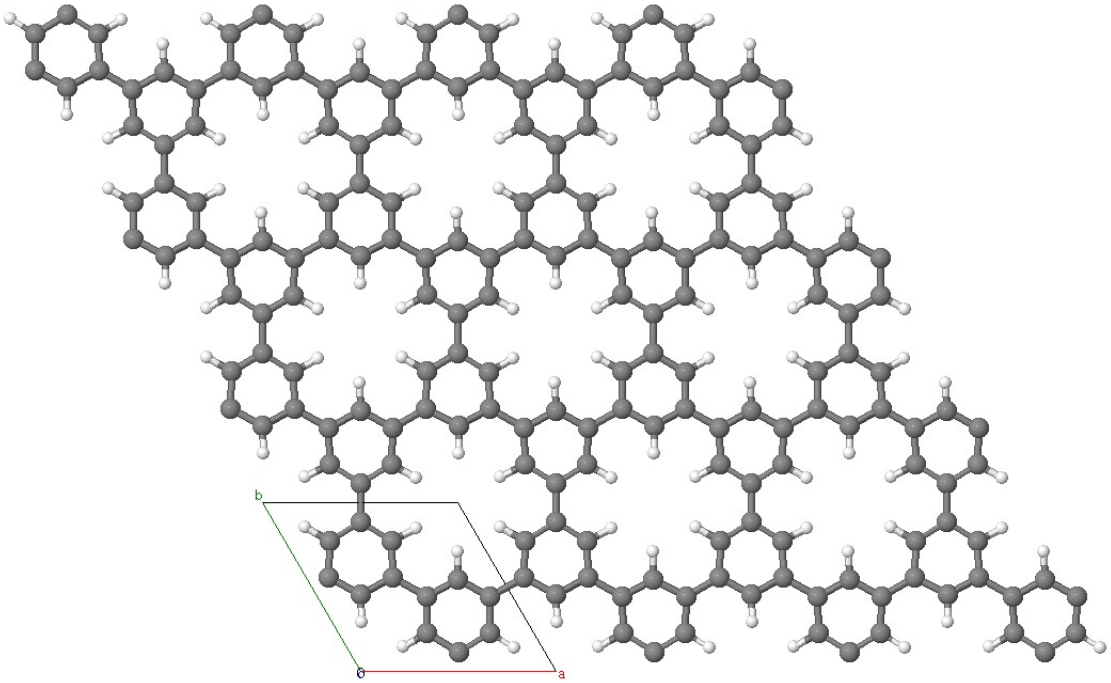

(a) HPG.

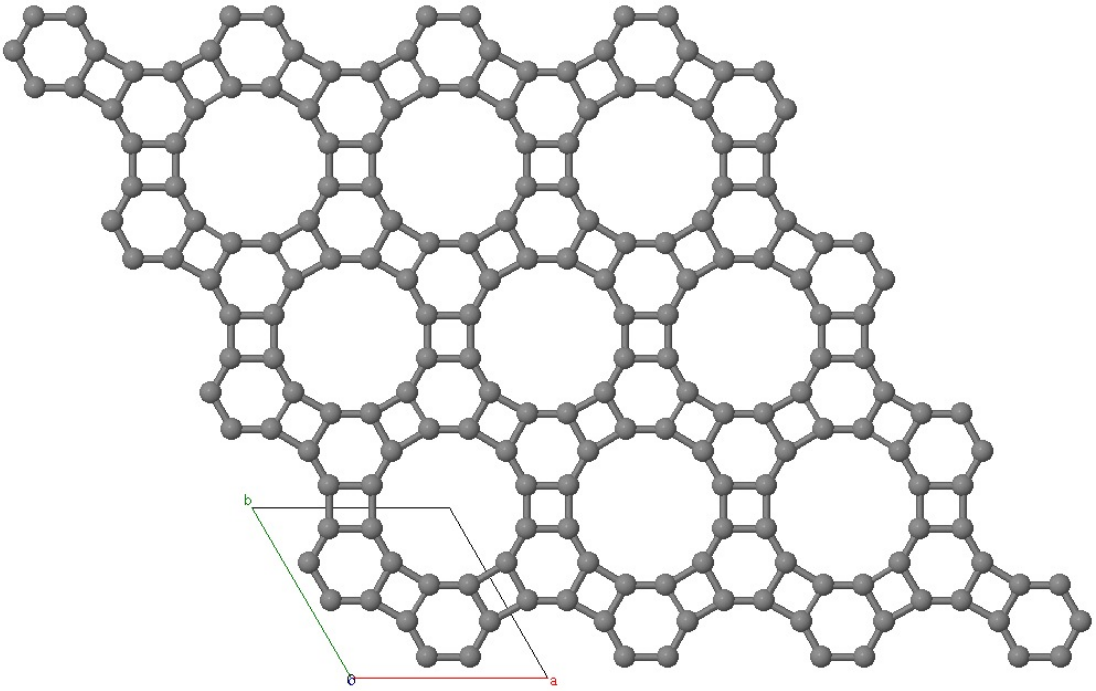

(b) BPC.

Figure 1: Planar view of 4x4 supercells of HPG and BPC.

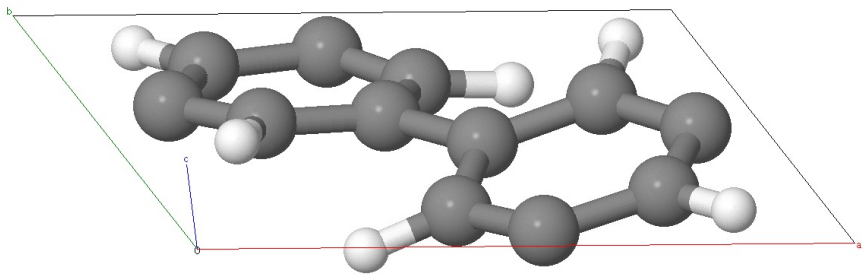

(a) HPG.

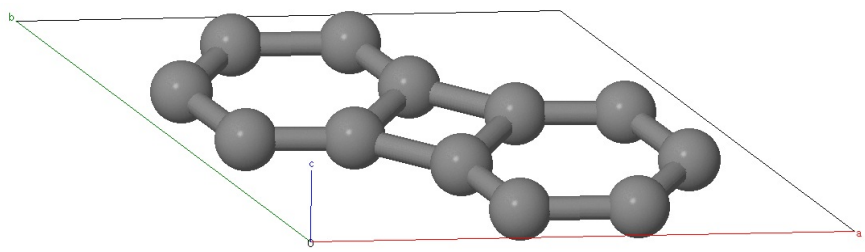

(b) BPC.

Figure 2: Perspective view of the unit cells for HPG and BPC. Note the tilting ($2\theta_{ring}$ = 20.9 degrees) between the two benzene-like rings in the HPG structure.

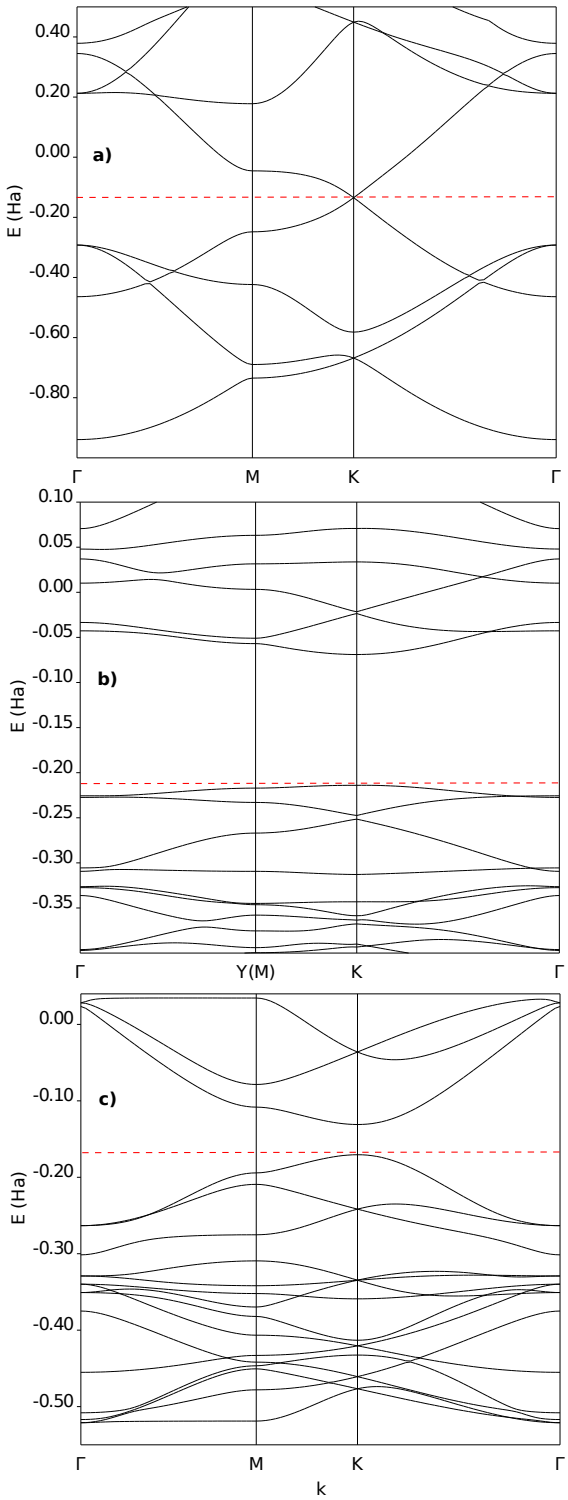

Figure 3: Computed electronic bands for a) graphene, b) HPG, c) BPC. Energies are in Ha (1 Ha = 27.211 eV). The Fermi level is indicated by a red dashed horizontal line. The direct band gap lies at the K point in all the three compounds. Due to lower symmetry, nomenclature for HPG is different (M is renamed to Y).

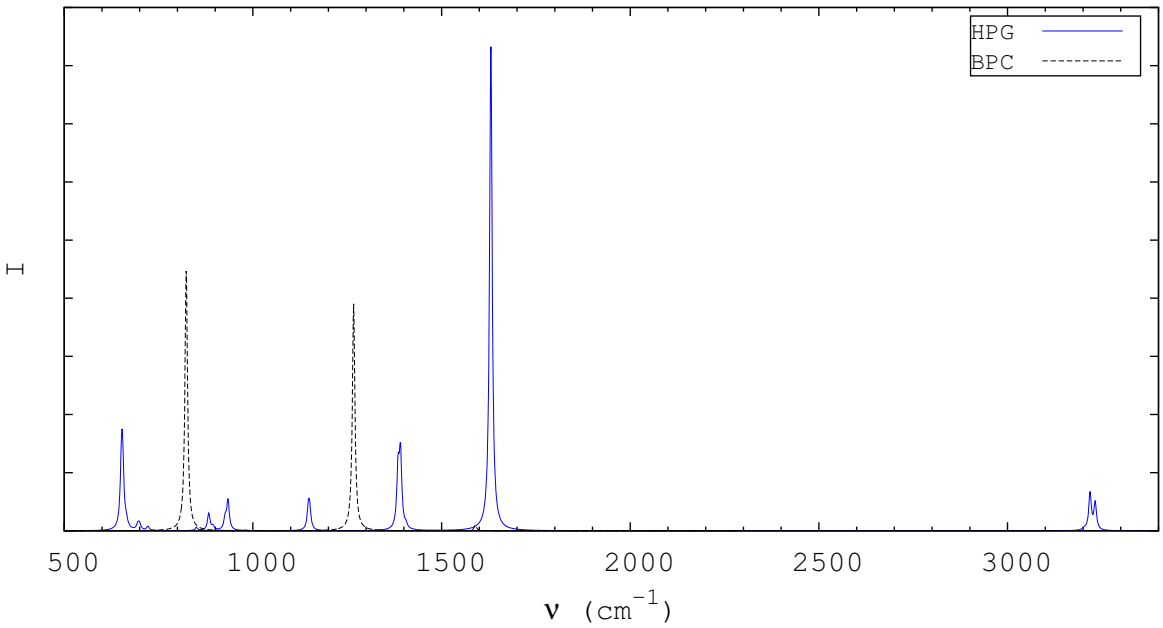

Figure 4: Computed IR spectra of HPG and BPC. The peak integrated intensity of each $n-th$ mode is II_n [km/mol] (see Table 3); details on the construction of the curves are given in Section 2.

Table 1: Structural and energetic parameters computed at the B3LYP level of theory. Lengths in Å, angles in degrees. θ_{ring} is the tilting angle between a benzene-like ring and the sheet plane; the tilting angle between pairs of rings is then $2\theta_{ring}$. In the case of graphene the cell parameter of a 3x3 supercell has been reported, for sake of comparison. In the case of multiple distances or angles, the minimum and maximum values are reported. ΔE [eV / C atom] for BPC is the energy difference with respect to graphene. For HPG, two values are given, corresponding to the hydrogenation energy of graphene with respect to molecular and atomic(*) hydrogen, respectively. Energy values are corrected for BSSE.

	graphene	HPG	BPC
SG	$P6/mmm$	$C222$	$P6/mmm$
a	7.3814	7.4632	6.7470
d_{C-C}	1.4218	1.3979	1.3562
		1.4924	1.4829
d_{C-H}	–	1.0795	–
d_{H-H}	–	1.9509	–
		2.0496	
θ_{C-C}	120.0	117.5	90.0
		122.6	150.0
θ_{C-H}	–	118.6	–
		119.5	
θ_{ring}	–	10.45	–
ΔE	–	+0.099	+0.658
	–	-1.097*	–

Table 2: Static electronic polarizability α [bohr^3], first hyperpolarizabilities β [atomic units] and second hyperpolarizabilities γ [atomic units] by using the B3LYP functional and a Gaussian-type basis set with ghost functions (BS D in Table 4). Data refer to the unit cells described in Table 1: in the case of graphene a 3x3 supercell is adopted, for sake of comparison. Values correspond then to 18 C atoms (graphene), 12 C plus 6 H atoms (HPG), 12 C atoms (BPC). E_g is the electronic direct band gap [eV] and is reported in the last row.

	graphene	HPG	BPC
α_{xx}	∞	324.24	719.17
α_{yy}	∞	332.30	719.17
α_{zz}	52.262	49.695	39.659
β_{xyz}	0.00	20.1	0.00
γ_{xxxx}	∞	$1.2610\cdot10^6$	$4.0985\cdot10^7$
γ_{yyyy}	∞	$1.5794\cdot10^6$	$4.0985\cdot10^7$
γ_{zzzz}	$2.56\cdot10^3$	$4.66\cdot10^3$	$2.80\cdot10^3$
γ_{xxyy}	∞	$4.8048\cdot10^5$	$1.3662\cdot10^7$
γ_{xxzz}	∞	$6.89\cdot10^3$	$8.04\cdot10^3$
γ_{yyzz}	∞	$7.26\cdot10^3$	$8.04\cdot10^3$
E_g	0.000	3.948	1.078

Table 3: Vibrational properties at the B3LYP level of theory. ν_0 are the frequencies [cm^{-1}], II are the integrated IR intensities [km/mol]; "Sym" columns reports the IRREP label. Raman activity of the modes for BPC is indicated in the corresponding column; note that for HPG all modes are Raman active. Frequencies of modes with intensity higher than 10 km/mol are in bold. Harmonic frequencies above 3000 cm^{-1} are C-H stretching modes; the estimated anharmonic correction is 106 cm^{-1}. Vibrational frequencies for graphene computed within the same computational framework are 756.3 (inactive) and 1607.7 (Raman active) cm^{-1}.

HPG						BPC			
Sym	ν_0	II	Sym	ν_0	II	Sym	ν_0	II	Raman
B1	43.4	0	A	1044.0		$E2_u$	223.9		
A	158.0		B3	1046.9	0	$B1_g$	229.6		
B2	222.2	0	B2	**1147.1**	23	$E1_g$	376.7		A
B3	240.7	0	B3	**1150.6**	19	$B2_u$	466.8		
B2	248.7	0	A	1232.0		$E1_g$	539.8		A
B2	345.7	0	B1	1246.1	0	$E2_g$	569.2		A
B1	448.1	0	B1	1308.4	0	$B2_g$	676.4		
A	458.5		B1	1317.1	0	$E2_u$	741.5		
B1	469.5	0	B2	1323.6	0	$A2_u$	794.6		
A	481.1		B3	**1384.7**	61	$E1_u$	**823.4**	283	
B1	640.0	0	B2	**1391.2**	78	$B1_u$	852.7		
B2	**651.9**	63	B2	1405.6	4	$A2_g$	905.4		
B3	**654.8**	61	A	1408.9		$A2_g$	947.3		
B2	664.8	6	A	1538.7		$A1_g$	1036.6		A
B3	694.9	6	B1	1546.1	0	$E2_g$	1123.6		A
B2	699.5	6	B3	**1630.2**	245	$E2_g$	1215.7		A
B1	721.7	4	B2	**1631.0**	287	$B1_u$	1229.1		
B1	850.1	3	B1	1639.7	0	$E1_u$	**1267.0**	245	
B1	**882.9**	19	A	1641.2		$B2_u$	1311.4		
B2	894.2	4	B3	3201.0	1	$E1_u$	1589.5	6	
A	915.7		B1	3205.1	1	$E2_g$	1747.7		A
B3	**926.5**	12	A	3210.0		$A1_g$	1756.1		A
B2	**934.0**	32	B2	**3218.5**	40				
A	979.8		B3	**3232.2**	30				
B1	981.2	1	A	3237.7					
B3	1010.0	0							

Table 4: Effect of the basis set (BS) on the static electronic polarizability α [bohr^3] and second hyperpolarizabilities γ [atomic units] of BPC. A) original 6-31G(2d) BS; B) BS A + 1 *s* ghost function at the center of the 12-C ring + 2 layers of *s* ghost functions (*z* distance from atomic slab: $\pm$1.5 Å); C) BS B + 2 layers of *s* ghosts (*z* distance $\pm$3.0 Å); D) BS C + 2 layers of *s* ghosts (*z* distance $\pm$4.5 Å). For each value, the percent difference with respect to the value computed with the next BS in the series is given in brackets. The last row reports the time [s] required to run the (hyper)polarizability calculation on a 24-core cluster (each core has a Intel Xeon 2.5 GHz CPU and 2 GB RAM).

	A		B		C		D
α_{xx}	696.67	(-3.2)	718.98	(0.0)	719.06	(0.0)	719.17
α_{zz}	28.060	(-39.8)	39.242	(-1.0)	39.640	(0.0)	39.659
γ_{xxxx}	$3.7314 \cdot 10^7$	(-9.8)	$4.0958 \cdot 10^7$	(0.0)	$4.0969 \cdot 10^7$	(0.0)	$4.0985 \cdot 10^7$
γ_{zzzz}	≈ 0	(—)	1401.0	(-72.0)	2409.9	(-16.0)	2795.6
γ_{xxyy}	$1.2438 \cdot 10^7$	(-9.8)	$1.3653 \cdot 10^7$	(0.0)	$1.3656 \cdot 10^7$	(0.0)	$1.3662 \cdot 10^7$
γ_{xxzz}	1252.3	(-480.0)	7263.1	(-7.7)	7825.4	(-2.7)	8038.7
t	9476		56618		150529		293284

References

(1) Novoselov, K. S.; Geim, A. K.; Morozov, S. V.; Jiang, D.; Zhang, Y.; Dubonos, S. V.; Grigorieva, I. V.; Firsov, A. A. *Science* **2004**, *306*, 666.

(2) Geim, A. K.; Novoselov, K. S. *Nature Mat.* **2007**, *6*, 183.

(3) Davey, S. *Nature Chem.* **25/09/2009**, 10.1038/nchem.415.

(4) Bieri, M.; Treier, M.; Cai, J.; Aït-Mansour, K.; Ruffieux, P.; Gröning, O.; Gröning, P.; Kastler, M.; Rieger, R.; Feng, X.; Müllen, K.; Fasel, R. *Chem. Commun.* **2009**, *45*, 6919.

(5) Novoselov, K. S.; Geim, A. K.; Morozov, S. V.; Jiang, D.; Katsnelson, M. I.; Grigorieva, I. V.; Dubonos, S. V.; Firsov, A. A. *Nature* **2005**, *438*, 197.

(6) Balandin, A. A.; Ghosh, S.; Bao, W.; Calizo, I.; Teweldebrhan, D.; Miao, F.; Lau, C. N. *Nano Lett.* **2008**, *8*, 902.

(7) Lee, C.; Wei, X.; Kysar, J. W.; Hone, J. *Science* **2008**, *321*, 385.

(8) Singh, V.; Joung, D.; Zhai, L.; Das, S.; Khondaker, S.; Seal, S. *Prog. Mater. Sci.* **2011**, *56*, 1178.

(9) Castro Neto, A. H.; Guinea, F.; Peres, N. M. R.; Novoselov, K. S.; Geim, A. K. *Rev. Mod. Phys.* **2009**, *81*, 109.

(10) Du, H.; Li, J.; Zhang, J.; Su, G.; Li, X.; Zhao, Y. *J. Phys. Chem. C* **2011**, *115*, 23261.

(11) Xiao, J.; Mei, D.; X. Li, W. X.; Wang, D.; Graff, G. L.; Bennett, W. D.; Nie, Z.; Saraf, L. V.; Aksay, I. A.; Liu, J.; Zhang, J. *Nano Lett.* **2011**, *11*, 5071.

(12) Du, A.; Zhu, Z.; Smith, S. C. *J. Am. Chem. Soc.* **2010**, *132*, 2876.

(13) Nair, R. R.; Wu, H. A.; Jayaram, P. N.; Grigorieva, I. V.; Geim, A. K. *Science* **2012**, *335*, 442.

(14) Baughman, R. H.; Eckhardt, H.; Kertesz, M. *J. Chem. Phys.* **1987**, *87*, 6687.

(15) Enyashin, A. N.; Ivanovskii, A. L. *Phys. Status Solidi B* **2011**, *248*, 1879.

(16) Brunetto, G.; Autreto, P. A. S.; Machado, L. D.; Santos, B. I.; dos Santos, R. P. B.; Galvao, D. S. *J. Phys. Chem. C* **2012**, *116*, 12810.

(17) Bonaccorso, F.; Sun, Z.; Hasan, T.; Ferrari, A. C. *Nature Photon.* **2004**, *4*, 611.

(18) Yamashita, S. *J. Lightwave Technol.* **2012**, *30*, 427.

(19) Wang, J.; Hernandez, Y.; Lotya, M.; Coleman, J. N.; Blau, W. J. *Adv. Mater.* **2009**, *21*, 2430.

(20) Wu, R.; Zhang, Y.; Yan, S.; Bian, F.; Wang, W.; Bai, X.; Lu, X.; Zhao, J.; Wang, E. *Nano Lett.* **2011**, *11*, 5159.

(21) Hendry, E.; Hale, P. J.; Moger, J.; Savchenko, A. K.; Mikhailov, S. A. *Phys. Rev. Lett.* **2010**, *105*, 097401.

(22) Kan, E.; Li, Z. Y.; Yang, J. L. *Nano* **2008**, *3*, 433.

(23) Xia, F.; Avouris, P. *IEEE Photon.* **2011**, *3*, 293.

(24) Dovesi, R.; Saunders, V. R.; Roetti, C.; Orlando, R.; Zicovich-Wilson, C. M.; Pascale, F.; Doll, K.; Harrison, N. M.; Civalleri, B.; Bush, I. J.; D'Arco, P.; Llunell, M. CRYSTAL09 User's Manual. 2009.

(25) Dovesi, R.; Orlando, R.; Civalleri, B.; Roetti, C.; Saunders, V. R.; Zicovich-Wilson, C. M. *Z. Kristallogr.* **2005**, *220*, 571.

(26) Becke, A. D. *J. Chem. Phys.* **1993**, *98*, 5648.

(27) Lee, C.; Yang, W.; Parr, R. G. *Phys. Rev. B* **1988**, *37*, 785.

(28) Stephens, P. J.; Devlin, F. J.; Chabalowski, C. F.; Frisch, M. J. *J. Phys. Chem.* **1994**, *98*, 11623.

(29) Noël, Y.; D'Arco, P.; Demichelis, R.; Zicovich-Wilson, C.; Dovesi, R. *J. Comput. Chem.* **2010**, *31*, 855.

(30) Demichelis, R.; Noël, Y.; D'Arco, P.; Rérat, M.; Zicovich-Wilson, C.; Dovesi, R. *J. Phys. Chem. C* **2011**, *115*, 8876.

(31) Orlando, R.; Bast, R.; Ruud, K.; Ekström, U.; Ferrabone, M.; Kirtman, B.; Dovesi, R. *J. Phys. Chem. A* **2011**, *115*, 12631.

(32) Ferrabone, M.; Kirtman, B.; Rérat, M.; Orlando, R.; Dovesi, R. *Phys. Rev. B* **2011**, *83*, 235421.

(33) Ferrabone, M.; Kirtman, B.; Lacivita, V.; Rérat, M.; Orlando, R.; Dovesi, R. *Int. J. Quantum Chem.* **2012**, *112*, 2160.

(34) Lacivita, V.; Rérat, M.; Kirtman, B.; Ferrero, M.; Orlando, R.; Dovesi, R. *J. Chem. Phys.* **2009**, *131*, 204509.

(35) Orlando, R.; Lacivita, V.; Bast, R.; Ruud, K. *J. Chem. Phys.* **2010**, *132*, 244106.

(36) Demichelis, R.; Civalleri, B.; Ferrabone, M.; Dovesi, R. *Int. J. Quantum Chem.* **2010**, *110*, 406.

(37) Lacivita, V.; Rérat, M.; Orlando, R.; Ferrero, M.; Dovesi, R. *J. Chem. Phys.* **2012**, *136*, 114101.

(38) Lacivita, V.; Rérat, M.; Kirtman, B.; Orlando, R.; Ferrabone, M.; Dovesi, R. *J. Chem. Phys.* **2012**, *137*, 014103.

(39) Karamanis, P.; Pouchan, C. *J. Phys. Chem. C* **2012**, *116*, 11808.

(40) Koukaras, E. N.; Zdetsis, A. D.; Karamanis, P.; Pouchan, C.; Avramopoulos, A.; Papadopoulos, M. G. *J. Comput. Chem.* **2012**, *33*, 1068.

(41) Karamanis, P.; Pouchan, C.; Weatherford, C. A.; Gutsev, G. L. *J. Phys. Chem. C* **2011**, *115*, 97.

(42) Doll, K. *Comput. Phys. Comm.* **2001**, *137*, 74.

(43) Doll, K.; Harrison, N. M.; Saunders, V. R. *Int. J. Quantum Chem.* **2001**, *82*, 1.

(44) Civalleri, B.; D'Arco, P.; Orlando, R.; Saunders, V. R.; Dovesi, R. *Chem. Phys. Lett.* **2001**, *348*, 131.

(45) Broyden, C. G. *J. Inst. Math. Appl.* **1970**, *6*, 76.

(46) Fletcher, R. *Comput. J.* **1970**, *13*, 317.

(47) Goldfarb, D. *Math. Comput.* **1970**, *24*, 23.

(48) Shanno, D. F. *Math. Comput.* **1970**, *24*, 647.

(49) Barrow, G. M. *Introduction to molecular spectroscopy*; McGraw-Hill, New York, 1962; Chapter 4, p 70.

(50) Hess, B. A.; Schaad, L. J.; Carsky, P.; Zahradnik, R. *Chem. Rev.* **1986**, *86*, 709.

(51) Dall'Olio, S.; Dovesi, R.; Resta, R. *Phys. Rev. B* **1997**, *56*, 10105.

(52) Baranek, P.; Zicovich-Wilson, C. M.; Roetti, C.; Orlando, R.; Dovesi, R. *Phys. Rev. B* **2001**, *64*, 125102.

(53) Noël, Y.; Zicovich-Wilson, C. M.; Civalleri, B.; D'Arco, P.; Dovesi, R. *Phys. Rev. B* **2002**, *65*, 014111.

(54) Pascale, F.; Zicovich-Wilson, C. M.; Gejo, F. L.; Civalleri, B.; Orlando, R.; Dovesi, R. *J. Comput. Chem.* **2004**, *25*, 888.

(55) Zicovich-Wilson, C. M.; Pascale, F.; Roetti, C.; Saunders, V. R.; Orlando, R.; Dovesi, R. *J. Comput. Chem.* **2004**, *25*, 1873.

(56) Zicovich-Wilson, C. M.; Torres, F. J.; Pascale, F.; Valenzano, L.; Orlando, R.; Dovesi, R. *J. Comput. Chem.* **2008**, *29*, 2268.

(57) Hurst, G. J. B.; Dupuis, M.; Clementi, E. *J. Chem. Phys.* **1988**, *89*, 385.

(58) Kirtman, B.; Gu, F. L.; Bishop, D. M. *J. Chem. Phys.* **2000**, *113*, 1294.

(59) Ferrero, M.; Rérat, M.; Orlando, R.; Dovesi, R. *J. Comput. Chem.* **2008**, *29*, 1450.

(60) Ferrero, M.; Rérat, M.; Orlando, R.; Dovesi, R. *J. Chem. Phys.* **2008**, *128*, 014110.

(61) Ferrero, M.; Rérat, M.; Kirtman, B.; Dovesi, R. *J. Chem. Phys.* **2008**, *129*, 244110.

(62) Ferrero, M.; Rérat, M.; Orlando, R.; Dovesi, R. *Coupled Perturbed Hartree-Fock Calculation of the static polarizability for periodic systems: implementation in the CRYSTAL code*; AIP Conference Proceedings; T. E. Simos and G. Maroulis, American Institute of Physics, 2007; Vol. Computation in Modern Science and Engineering, Volume 2B; pp 1199–1203.

(63) Orlando, R.; Ferrero, M.; Rérat, M.; Kirtman, B.; Dovesi, R. *J. Chem. Phys.* **2009**, *131*, 184105.

(64) Kirtman, B.; Lacivita, V.; Dovesi, R.; Reis, H. *J. Chem. Phys.* **2011**, *135*, 154101.

(65) Dovesi, R.; De La Pierre, M.; Ferrari, A. M.; Pascale, F.; Maschio, L.; Zicovich-Wilson, C. M. *Am. Mineral.* **2011**, *96*, 1787–1798.

(66) Du, A.; Zhu, Z.; Smith, S. C. *J. Am. Chem. Soc.* **2010**, *132*, 2876.

(67) Tomić, S.; Montanari, B.; Harrison, N. M. *Physica E* **2008**, *40*, 2125.

(68) Matsuda, Y.; Tahir-Kheli, J.; Goddard III, W. A. *J. Phys. Chem. Lett.* **2010**, *1*, 2946.

(69) Civalleri, B.; Presti, D.; Dovesi, R.; Savin, A. In *Chemical Modelling*; Springborg, M., Ed.; R. Soc. Chem., 2012; Vol. 9; p 168.

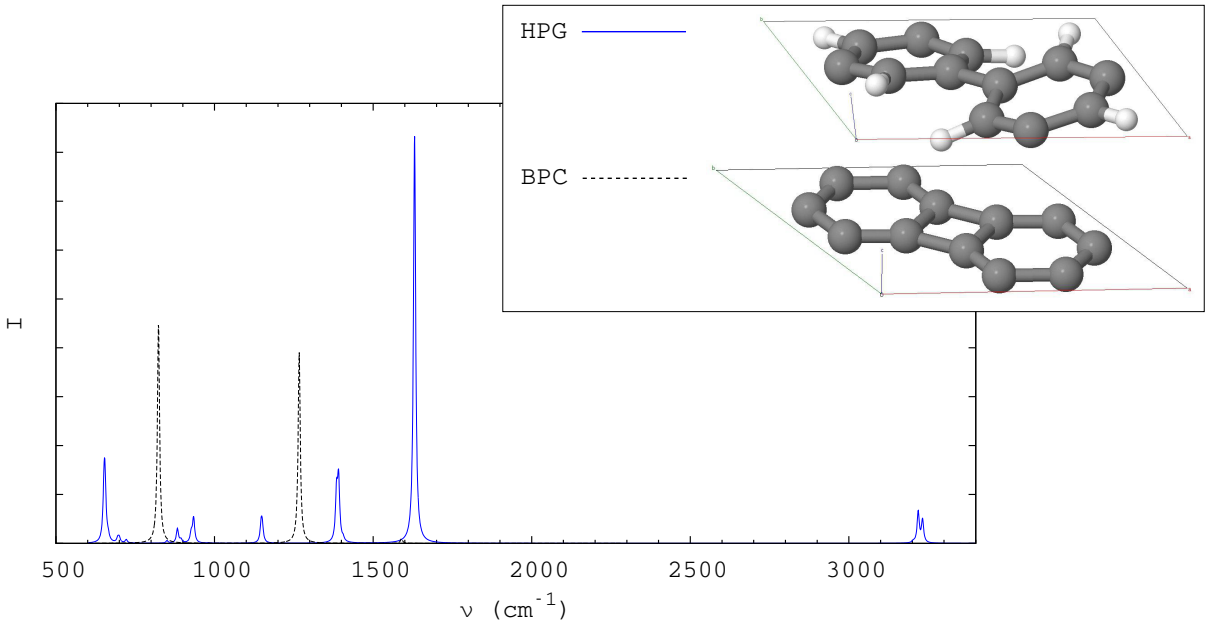

Figure 5: TOC - Graphical Abstract